Identification of High-Temperature Exciton States and Their Phase-Dependent Trapping Behaviour in Lead Halide Perovskites

Journal:	*Energy & Environmental Science*
Manuscript ID	EE-ART-12-2017-003543.R1
Article Type:	Paper
Date Submitted by the Author:	02-Mar-2018

Complete List of Authors:	Shi, Jiangjian; Institute of Physics, Chinese Academy of Sciences, Zhang, Huiyin; Institute of Physics, Chinese Academy of Sciences, Li, Yiming; Institute of Physics, Chinese Academy of Sciences Jasieniak, Jacek; Monash University, Materials Science and Engineering Li, Yusheng; Institute of Physics, Chinese Academy of Sciences Wu, Huijue; Institute of Physics,Chinese Academy of Sciences, Luo, Yanhong; Institute of Physics, Chinese Academy of Sciences, Beijing National Laboratory for Condensed Matter Physics Li, Dongmei; Institute of Physics, Chinese Academy of Sciences, Beijing National Laboratory for Condensed Matter Physics Meng, Qingbo; Institute of Physics, Chinese Academy of Sciences,

Journal Name

ARTICLE

Identification of High-Temperature Exciton States and Their Phase-Dependent Trapping Behaviour in Lead Halide Perovskites

Received 00th January 20xx,
Accepted 00th January 20xx

DOI: 10.1039/x0xx00000x

www.rsc.org/

Jiangjian Shi[a], Huiyin Zhang[a, c], Yiming Li[a, c], Jacek J. Jasieniak[b*], Yusheng Li[a, c], Huijue Wu[a], Yanhong Luo[a, c], Dongmei Li[a, c], Qingbo Meng[a, c*]

While lead halide perovskites have rapidly emerged as lucrative material candidates for optoelectronic applications, the crucial energy states and charge-carrier nature of these systems are yet to be fully understood, resulting in ongoing debates on the fundamental optical and material character. In this work we probe the band-edge and sub-gap energy states within polycrystalline and single crystal perovskites to better understand their photophysical origins. Through temperature-, excitation intensity- and time-dependent optical measurements, we reveal the existence of both free and bound exciton contributions to the optoelectronic properties across a wide temperature region up to 300 K. The low-energy absorption and multiple-peak emission phenomena, whose physics origins have been in highly controversial before, are caused by these exciton states. Furthermore, the trapping and recombination dynamics of these excitons is shown to be strongly dependent on the structural phase of the perovskite. The orthorhombic phase exhibits an ultrafast exciton trapping and distinct trap emissions, while the tetragonal phase gives low monomolecular recombination velocity and capture cross-sections (~10^{-18} cm^2). Within the multiphonon transition scenario, this suppression in charge trapping is caused by the increase in the charge capture activation energy due to a reduction in electron-lattice interactions within the inorganic framework, which can reasonably interpret the unexpectedly long carrier lifetime in these material systems. These findings provide a clearer understanding into the origins of the photophysical properties of perovskite materials, and the discovery of a high-temperature-stable bound exciton would bring the excitonic feature to be a concern for the perovskite energy conversion and utilization applications.

Introduction

Hybrid metal halide perovskites have rapidly emerged as promising materials for use within high-efficiency photovoltaic,[1-5] light-emitting,[6-7] and detecting[8] devices. These successes have arisen because of the outstanding optoelectronic properties that such materials possess, including high light absorption coefficients (α) of >10^5 cm^{-1} across the visible region,[9-10] long carrier lifetimes that can exceed 1 μs,[11-13] and unexpectedly slow hot-carrier cooling processes.[14-15] Underlying these alluring characteristics is an intrinsic photophysical mechanism that dictates the absorption of light, carrier thermalization and cooling, and recombination or charge-transfer dynamics.[16-17]

Recent studies have highlighted the importance of a hot-phonon bottleneck and polaron screening effects towards explaining the excited state carrier dynamics in these materials.[14-15] Following cooling, reports have suggested that free carrier formation dominates at high temperatures,[18-19] while excitonic contributions, which include resonance,[20] localization,[21] and transfer,[22] were also reported. The band-edge light absorption of perovskites has been attributed to these exciton states;[23] however, contrasting reports have also suggested that this arises from band-tail states or indirect band transitions.[24, 25] An indirect bandgap model has most recently been invoked to describe the band-edge bimolecular recombination in these systems.[26] It is evident that low-energy electronic states within the direct band edge of perovskites play a fundamental role in defining their optoelectronic properties.[27] The importance of such states is confirmed with studies showing that the trap-mediated charge capture dominates the recombination dynamics,[19] while also accelerates ion migration and performance degradation.[28-30] However, little convincing consensus about these energy states has been obtained, resulting in ongoing debates on the fundamental optical and material characters, e.g., the low-energy absorption in single crystals[23, 31-32], ultra-long carrier cooling and recombination lifetime,[14-15] excitonic-free carrier features,[18-22] and direct-indirect bandgap characters.[25-26]

Herein, we study the band-edge and sub-gap energy state related absorption and fluorescence characteristics of methylammonium lead halide perovskites (including

[a] Key Laboratory for Renewable Energy, Chinese Academy of Sciences; Beijing Key Laboratory for New Energy Materials and Devices; Institute of Physics, Chinese Academy of Sciences, Beijing 100190, P. R. China.
[b] Department of Materials Science and Engineering, Monash University, Clayton, Victoria 3800, Australia
[c] University of Chinese Academy of Sciences, Beijing 100049, P. R. China.
* **Corresponding author:** qbmeng@iphy.ac.cn, jacek.jasieniak@monash.edu
Electronic Supplementary Information (ESI) available. See DOI: 10.1039/x0xx00000x

$CH_3NH_3PbBr_3$ ($MAPbBr_3$) and $MAPbI_3$) to better understand their photophysical origins. Through temperature-, excitation intensity- and time-dependent measurements, we find explicit signatures of a free and bound exciton in both polycrystalline and single crystal samples across a wide temperature region up to 300 K. These exciton states play a critical role in determining the band-edge absorption characteristics and in causing the multiple emission phenomena. The spectral dynamics of these excitons exhibit a phase-dependent behaviour, with the orthorhombic-to-tetragonal phase transition effectively prohibiting exciton trapping. Within the multiphonon transition theory, this behaviour is found to originate from an increase of the trap capture activation energy following the phase transformation. These findings provide a clearer understanding into the origins of the photophysical properties of perovskite materials, which also bring direct implications towards the energy state regulations for improved perovskite device and energy applications.

Results and Discussion.

A. Low-energy absorption and multiple emissions in polycrystalline perovskites caused by free and bound excitons.

Studies on the low-energy absorption of perovskites have shown that a bathochromic shift occurs when the perovskite is grown from as a polycrystalline thin-film through to a single crystal.[23, 31-32] The diversity of exciton states at the crystal surface and in the bulk have been suggested to be the origin for this phenomenon.[23] However, these propositions have not adequately considered the potential variation in defect density, lattice ordering, and perovskite thickness across these samples, which can readily obscure the underlying cause of any absorption edge changes. To exclude these effects, we have selectively used polycrystalline samples of a common origin for this study. $MAPbBr_3$ was chosen as the representative perovskite sample because its absorption edge and emission are in the visible-region, and its orthorhombic-to-tetragonal phase transition occurs at a sufficiently low temperature[21] of ~140 K to decouple phase-related and intrinsic characteristics. Experimental results for the $MAPbI_3$ are also given in the Supplementary material as a point of reference. The $MAPbBr_3$ polycrystalline were grown by direct precipitation within a viscous ethylacetate (EA)/ethylcellulose (EC) solution to form a concentrated perovskite dispersion. The average size of perovskite grains within the dispersion is estimated to be ~ 400 nm by using light scattering (Supplementary Figure 1). This dispersion could be readily diluted through additional EA/EC; thus, enabling the perovskite concentration to be continuously adjusted, while preserving its underlying physical and chemical nature.

Measurements of the absorption characteristics of these perovskite dispersions at different concentrations are shown in Figure 1(a), which exhibit progressively more prominent low-energy optical features at higher concentrations. An analysis of this low-energy absorption edge as a function of perovskite concentration reveals a linear relationship (Figure 1b), consistent with the Beer-Lambert Law. These simply state that the extended absorption edge in these samples is arisen from electronic states that are intrinsic to each perovskite crystal in the sample. This similarity in the electronic states is further supported by the same emission properties of these samples (Supplementary Figure 2). Quantifying these states would provide a clearer physics image of the band-edge energy structure.

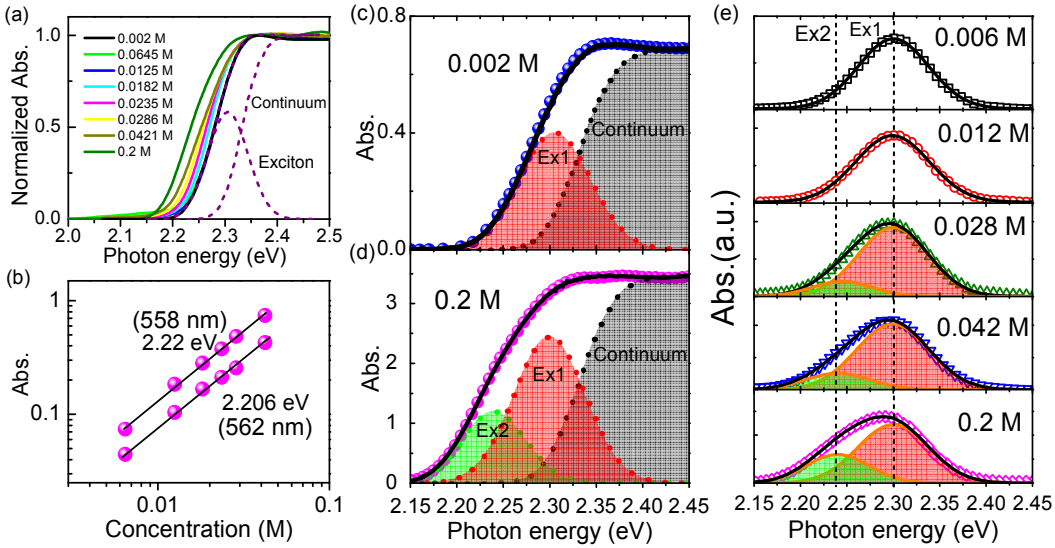

Figure 1. Light absorption and emission properties of the $MAPbBr_3$ dispersions at different concentrations. (a) Normalized light absorption spectra and (b) the low-energy light absorption as a function of the concentration. (c) and (d) give the full fits for the samples with 0.002 M and 0.2 M perovskite concentration, respectively. (e) The evolution of the exciton absorption when increasing the perovskite concentration. For clarity, the continuum-band term has been subtracted from the spectra.

Exciton, band-tail, and indirect-band states can all act as band-edge energy states that contribute to the optoelectronic properties at the absorption edge.[16] To quantify these contributions, we first considered the conventional Tauc formalism,[25] which is usually

composed of indirect (E_{ig}) and direct (E_g) bandgap terms scaled by proportionality factors a and b, respectively: $\alpha(E)=a\times(E-E_{ig})^2+b\times(E-E_g)^{1/2}$. However, this approach is proved unrealistic for perovskites, predicting them to be indirect semiconductors (Supplementary Figure 3). A more suitable approach to extract the absorption-related energy states involved the Elliott formula, which considers the continuum-band and excitonic contributions concurrently:[33]

$$\alpha(E)=\left[A\cdot\theta(E-E_g)\cdot D_{CV}(E)\right]\cdot\left[\frac{\pi x e^{\pi x}}{\sinh(\pi x)}\right]+A\cdot R_x\cdot\sum_{n=1}^{\infty}\frac{4\pi}{n^3}\cdot\delta\left(E-E_g+R_x/n^2\right) \quad (1)$$

where A is a constant, E is the photon energy, θ is the step function, D_{CV} is the joint density of states described as $D_{CV}\sim(E-E_g)^{1/2}$ near the direct band edge, n is the principal quantum number of the exciton state, δ represents a delta function, and $x=[R_x/(E-E_g)]^{1/2}$, with R_x being the exciton binding energy.

Using the Elliot formalism, with a Gaussian broaden exciton contribution, the absorption spectrum of the 2 mM perovskite is fitted to yield an E_g of 2.32 eV and an R_x of ~20 meV (Figure 1(c)). This E_g is similar to that reported by Wu et al. for the $MAPbBr_3$ single crystal, while the R_x is much smaller than the ~60 meV found.[23] Considering the thermal energy at room temperature is ~26 meV, an exciton with a binding energy of only 20 meV can be considered to exist as a dissociated or free exciton. This free exciton has been widely reported in previous works.[14, 34] For the 0.2 M perovskite, evidently the absorption is extended to lower energy, but it cannot be adequately fitted by solely considering the continuum-band and single exciton transition (Supplementary Figure 4). Instead, we find that the Elliot formalism modified to include a secondary, low-energy Gaussian-shaped absorption band that is centred at ~2.245 eV provides an excellent fit to the experimental results (Figure 1(d)). Assuming a constant continuum and exciton contribution between the diluted and concentrated samples, we determine a binding energy for this additional resonance of ~ 75 meV.

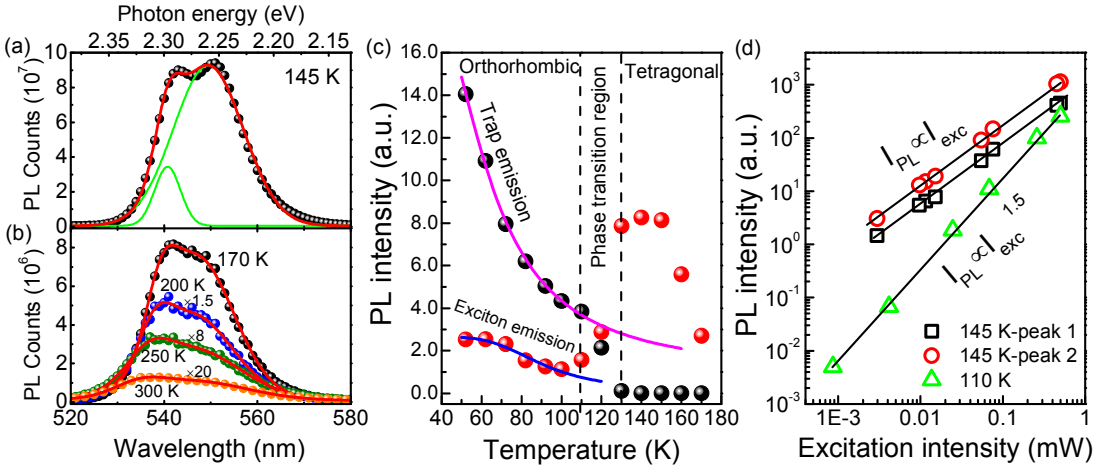

Figure 2. Temperature-dependent steady-state PL spectra of the $MAPbBr_3$ films. Experimentally measured and fitted PL spectra at (a) 145 K and (b) 170 K, 200 K, 250 K and 300 K. (c) Temperature-dependent exciton (free and bound excitons represented as an average) and trap emission intensities. In the low temperature regime of < 120 K, the relationships are fitted with the thermal quenching model. (d) Excitation intensity (I_{exc}) dependent exciton PL intensity (I_{PL}) of the perovskite at 110 K and 145 K, respectively. The data are fitted with $I_{PL}\sim I_{exc}^{c}$, which at 145 K gives $c\approx1$ for each of the two emission peaks and at 110 K gives $c\approx1.5$. For all the measurements, the perovskite was excited at 445 nm with an averaged excitation intensity of about 50 mW cm^{-2}.

The absorption tail below 2.22 eV can also be described by the indirect bandgap model (Supplementary Figure 4), which yields an E_{ig} of 2.138 eV. However, this model cannot provide a satisfactory global fit to the absorption spectra and is not consistent with the PL results (*vide infra*). In addition, because of the ultra-low absorption coefficient,[24-25] the exponential band tail (Urbach model) also cannot be used to explain the absorption characteristics here. Based on the above observations, we argue that the emerging low-energy absorption contribution in our $MAPbBr_3$ originates from another exciton state, which has a higher binding energy of up to 75 meV and, thus, can be considered as a bound exciton. The binding energy of this exciton bound to its host trap centre is about 55 meV, much higher than the average thermal energy (26 meV), thus sustaining its stability at room temperature.

In Figure 1(e) we show fitted absorption curves of all the samples with the continuum-band term subtracted for clarity. These results clearly show that the low-energy bound exciton absorption resonance becomes more evident at higher perovskite concentrations. Importantly, for all the perovskites, the free exciton resonances are located at the same position of ~ 2.30 eV and with a similar Gaussian broadening of ~ 38 meV. This is also the case for the bound exciton state, which always locates at ~2.245 eV with a broadening of ~ 33 meV. A similar behaviour is observed for $MAPbI_3$ samples, with two exciton states of binding energy 17 meV and 67 meV, respectively, being observed within the bandgap (E_g=1.645 eV, Supplementary Figure 5). Investigations into single crystal perovskites have also implied multiple exciton contributions for which the low-energy (high energy) contribution was assigned to the bulk (surface) of the perovskite single crystal.[23] Our results on

the polycrystalline samples suggest that it is difficult to validate whether these exciton states, especially the bound one, originate from the surface or the bulk. It is possible that these two types of exciton states are intrinsic to the perovskite material. Although the double exciton states have been suggested by the observation of femtosecond four wave mixing (FWM) at temperatures lower than 40 K,[35] their small binding energy variation of 16 meV as found is more likely caused by the local potential fluctuation induced exciton localization.[21] Based on a comparison to these and other studies, we believe that we are the first to confirm the coexistence of free and bound exciton states at room temperature.

We further carried out steady-state photoluminescence (PL) on perovskite films (Supplementary Figure 6) as a function of temperature from 10 K to 300 K. At temperatures lower than 130 K, a sharp PL peak centred at about 550 nm is observed, along with a broad emission band centred at about 620 nm (Supplementary Figure 7). These can be assigned to exciton and trap emissions, respectively.[36] At higher temperatures, the trap emission disappears and the exciton emission is significantly enhanced. Moreover, at 145 K, two PL peaks located at 541 nm (2.292 eV) and 550 nm (2.255 eV) are distinguished in the PL spectrum (Figure 2(a)). The energies of these PL peaks are similar to that of the free and bound exciton states, respectively, which may imply the successful observation of free and bound exciton emissions also at these temperatures. Notably, the PL of an $MAPbI_3$ film at high temperatures is also contributed from two bands (Supplementary Figure 5 and 8), implying a similar origin.

In addition to surface and bulk origins,[23] it has been proposed that a double-peak emission in perovskites can result from a mixture of perovskite phases (orthorhombic and tetragonal) [37] as well as singlet and triplet state emission.[38] To probe the underlying origin in more detail, we measured the PL at much higher temperatures. The double-peak emission can be observed from 145 K all the way through to room temperature (Figure 2(b)); while for the $MAPbI_3$, this can also be observed at room temperature (Supplementary Figure 5). At these high temperatures, phase pure samples should be expected. Further evidence for this is garnered through a comparison of the temperature (T)-dependent PL intensity ($I_{PL}(T)$) (Figure 2(c) and Supplementary Figure 9). At temperatures lower than 110 K, both the intensities of exciton and trap emissions decrease with temperature, following an Arrhenius thermal quenching model.[39] A dramatic decrease in the trap emission intensity is observed at temperatures beyond the 110 K, with a concurrent enhancement of the exciton emission being noted. This behaviour deviates from the thermal quenching model, thus implying a change in the emission mechanism across different temperature regimes, which is directly correlated to the internal phase of the material. Further analysis of the excitation intensity (I_{exc}) dependent PL measurements (Figure 2(d)) shows that at 110 K, the exciton PL intensity changes according to the power relationship $I_{PL} \sim I_{exc}^{c}$ (ref. 40-41) with $c \approx 1.5$. However, at 145 K, a linear relationship (i.e. $c \approx 1$) is obtained for each of the two emission peaks, indicating a different charge transfer and dynamic process.[41] These trends in PL behaviours suggest that the orthorhombic phase participating in the luminescence has been completely transformed into the tetragonal phase at temperatures higher than 130 K. Notably, it was previously reported that the multiple-peak PL observed at 50 K in such systems is arisen from singlet and triplet exciton emissions;[38] however, based on the excitation intensity induced PL peak blue-shift, it is more likely to arise from trap states.

B. Excitons at the surface and exposed bulk of perovskite single crystals.

Polycrystalline perovskite powders and films could possess inherent inhomogeneity due to the existence of grain boundaries and lattice disorder.[36] To better understand the origins of the multiple PL contributions, we have grown $MAPbBr_3$ single crystals by an inverse temperature crystallization method,[42] which preferentially exposes the cubic (100) plane (Supplementary Figure 10). We carefully cleaved the single crystal to expose the bulk lattice. As once reported,[43] lattice reconstructions below the first atomic layer of the cleaved surface are reasonably ignored here. Short-wavelength excitation within a reflection-mode collection geometry was used to measure the emission wavelength-dependent PL transients of both as-prepared and cleaved surface regions. The resulting two-dimensional pseudocolor plots of these transient PL spectra are shown in Figure 3(a) and 3(b) for 165 K. Both samples show two emission centres located at about 542 nm (~2.29 eV) and 554 nm (2.24 eV), which are consistent with that observed in the polycrystalline perovskite samples. This double-peak emission can also be observed when the temperature is increased to 200 K (Supplementary Figure 11). Notably, light-scattering contributions[32] were ruled out as a possible cause of this double-peak emission in the single crystal PL based on different decay rates for each emission band (Supplementary Figure 12). Thus, we suggest that the free and bound exciton states also coexist within both the surface and bulk of the perovskite single crystal.

The wavelength dependent PL spectra at different decay times following excitation have been extracted from the two-dimensional pseudocolor plots (Figure 3 (c) and (d)). The free exciton emission contribution shows a slight red-shift by about 17 meV in the early decay stage, while the position of the bound exciton emission remains unchanged. This implies that the free exciton progressively relaxes into lower energy states with a localization energy of about 17 meV, while the bound exciton is more energetically stable. This exciton localization state rather than the discrete bound exciton may be the origin for the observed lower-energy FWM signal.[35] In addition, this red shift could result from the diffusion of the free exciton within the single crystal and the photon reabsorption; while the stabilization of the 554-nm-emission band indicates that this exciton is immobilized in the real space, thus supporting our bound exciton hypothesis. Furthermore, it is observed that the relative PL intensity of the bound exciton for the single crystal surface is much higher than that for the bulk. Usually, a bound exciton is formed due to the coulomb interaction between an exciton and a trap centre.[16] The greater existence of these states may imply that the trap density of the single crystal surface is much higher than that in the bulk.

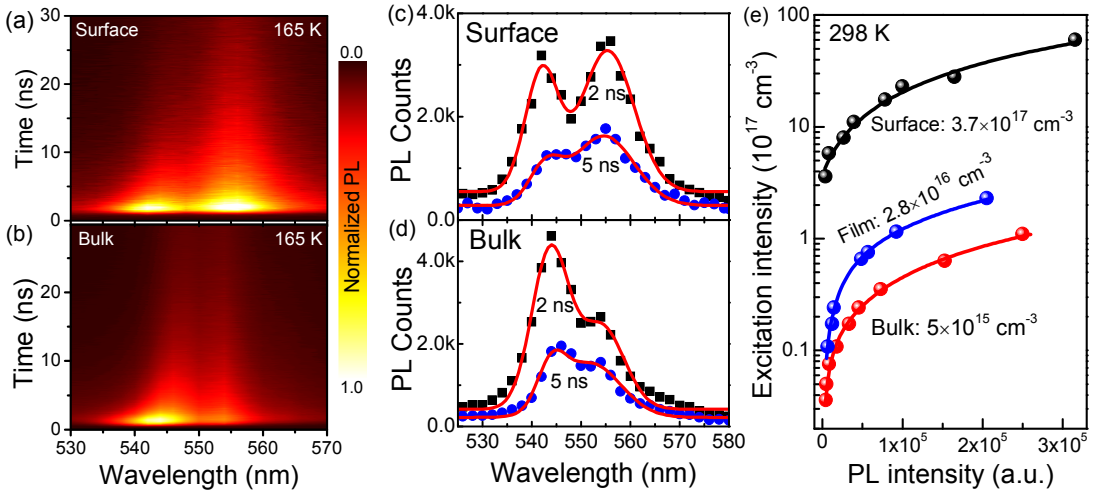

Figure 3. PL of the perovskite single crystal. Two dimensional pseudocolor (normalized PL intensity) plots of transient PL for the $MAPbBr_3$ single crystal as functions of emission wavelength and time delay (165 K, (a) surface and (b) bulk). The bulk is obtained by cleaving the single crystal and it is protected by a thin PMMA layer. Typical PL spectra of the perovskite single crystal at time delays of 2 and 5 ns, respectively ((c) surface and (d) bulk). These PL spectra are fitted with a double-peak emission model. (e) Trap density measurements of the perovskite by monitoring the pump density-dependent integrated PL intensity at room temperature.

To make such a correlation, the trap density of the perovskite single crystal (surface and bulk) and film is estimated using excitation intensity-dependent PL measurements (Figure 3(e)). According to the semiconductor band-edge recombination model,[7,23] these experimental dependences can be fitted by using $n(0)=N_t[1-\exp(-a\tau_0 I_{PL}/k)]+I_{PL}/k$, where $n(0)$ is the initial photocarrier density, N_t is the trap density, k is a constant for a certain sample, τ_0 is the effective PL lifetime, and a is the product of the trap capture cross section (σ) and the thermal velocity (v_{th}). To generate a relatively fast band-edge radiative rate for satisfying this model, this measurement was conducted at room temperature. Under this formalism, the trap density of the single crystal surface is estimated to be 3.7×10^{17} cm^{-3}, which is about two orders of magnitude higher than that of the bulk (5×10^{15} cm^{-3}). This result agrees well with the two-photon measurement[23], implying that the crystal quality (e.g. lattice ordering and defect) of the bulk perovskite have not been affected by the cleaving process. The correlation between the trap density and the bound exciton emission indicates that regulating the level of traps is necessary for charge localization for efficient perovskite emitting and lasing applications. Furthermore, a comparison of the PL characteristics of the perovskite films and single crystals, both at the surface and the exposed bulk, show similar behaviour (Supplementary Figure 13). This suggests that comparable energy states exist across the different perovskite samples we have studied.

Based on a PL lifetime for the polycrystalline perovskite films of ~ 350 ns (Supplementary Figure 14) at 300 K, the σ is estimated to be about 3.4×10^{-18} cm^2. Comparable values of σ were determined for other perovskite systems, such as the $MAPbI_3$ and (FA, MA)Pb(I, $Br)_3$. Impressively, these values are several orders of magnitude smaller than that for most traps in GaAs[44] and CdTe[45]. The small σ explains the origin for the unexpected slow monomolecular recombination in this material, but the physics mechanisms behind it deserve further studies.

C. Multiphonon transition-assisted exciton trapping and phase dependence.

Despite the low σ, we find that the excitons can be rapidly captured by trap states at low temperatures (Schematically depicted in Supplementary Figure 15). This can be readily observed at 70 K, for which three emission centres exist: free excitons, bound excitons, and radiative traps (Figure 4(a)). For clarity, the time for the PL maxima at different wavelengths are marked out by a black line and the transient PL probed at 545 nm and 620 nm is extracted and shown in Figure 4(b). The exciton emission exhibits an instrument-limited fast rise and sharp drop behaviour in the early stage; while for the trap emission, its rise process is much slower with no rapid drop being observed. A time delay of about 800 ps exists between these two types of emissions. The matching of the dynamics between the exciton emission decay and the concomitant rise of the trap emission implies the possibility of ultrafast charge transfer from exciton to trap states, i.e. exciton trapping. The transient PL for both the free and bound excitons is given in Supplementary Figure 16, and they exhibit a similar capture behaviour. Interestingly, at 170 K (tetragonal phase), the rapid drop of the exciton emission is no longer observed and the trap emission also disappears (Figure 4(b) and 2(c)). This behaviour deviates from the thermal quenching model, where a higher temperature would accelerate the exciton transfer (Supplementary material note 1).[39] These results indicate that the phase transition prohibits the rapid trapping of excitons. Notably, the hot carrier cooling process also exhibits a phase-dependent prohibition behaviour,[15] implying a potential correlation between these two dynamic processes.

The charge trapping process usually involves many-body interactions between electrons and phonons. It has been found that electron-phonon coupling makes significant contributions to the emission broadening[46] and charge transport scattering[47] within perovskites. Importantly, it was indicated that the orthorhombic-to-tetragonal phase transition would not induce significant changes to

the phonon spectra,[48] the carrier-phonon scattering rate,[47] or the phonon energy.[46] Thus, the phase-dependent exciton trapping behaviour is unlikely to be caused by phonon variations and more likely to be related to the underlying electronic properties. An indirect bandgap scenario has been put forward to explain the slow and temperature-dependent second-order recombination of perovskites.[26] However, it is difficult for this model to explain the observed ultra-low trap capture cross-sections, particularly since the trap states are usually non-localized in the *k*-space, and there is little evidence of an indirect bandgap nature. In addition, no obvious differences in the Rashba splitting were found for different perovskite phases,[49] suggesting that a direct-indirect bandgap transition also does not accompany the phase transition.

Inspired by the multiphonon transition theory for solids and semiconductors,[44, 50] here we propose that the phase transition may influence the electronic potential of the point trap in the lattice-coordinate (Q) space by changing the coupling between the continuum band and trap states (see Figure 4(c) and Supplementary material note 2). In the non-radiative charge capture process, the total energy (U) is distributed between electronic and lattice contributions (U=electronic + elastic energy). The charge transfer has to occur through the state coupling point Q_O with an energy barrier of $E_{B(O)}$ - the energy difference between the bottom of the conduction band and the state coupling point. The phase transition would change the lattice symmetry, atom spacing, and rotational freedoms.[51-52] These changes in atomic and lattice structure have been shown to decrease the elastic constants of perovskites after phase transition,[53] indicating a reduction of the electron-lattice interaction. This would cause a trap state in Q space to shift from $U_{t(O)}$ to $U_{t(T)}$, while also shifting the state coupling point to a higher energy position (Q_T).[44, 50] The charge capture energy barrier is thus increased to $E_{B(T)}$, which would significantly reduce the charge capturing probability. This model provides a qualitative and self-consistent explanation for the phase-dependent exciton trapping behaviour, but further experimental support is needed to verify its applicability.

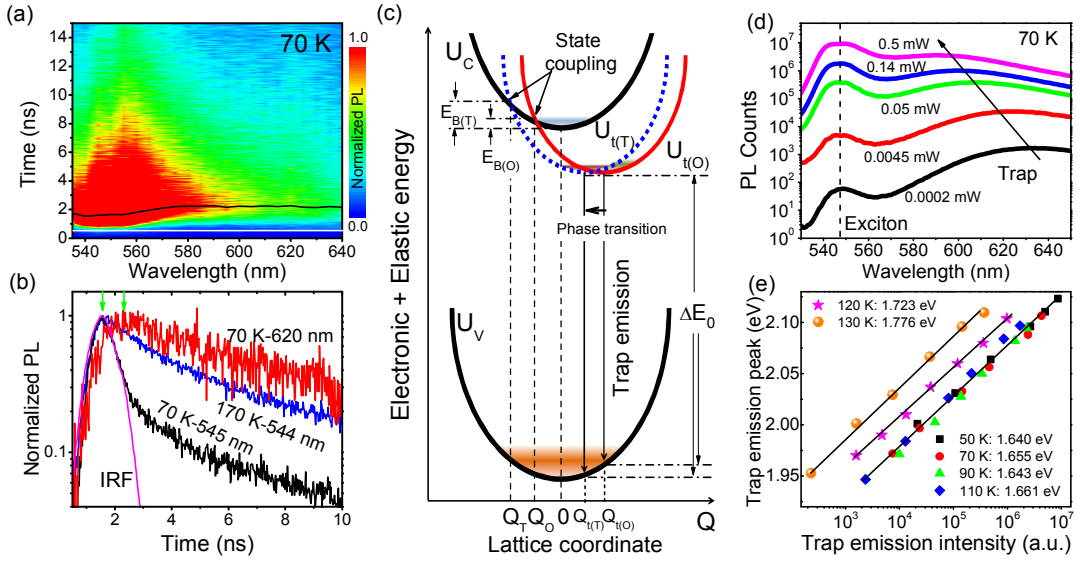

Figure 4. Exciton capture and trap emission of the perovskite at low temperatures. (a) Two dimensional pseudocolor (normalized PL intensity) plots of transient PL as functions of emission wavelength and time delay at 70 K. The black line marks out the time of the PL maximum at different wavelengths. (b) Transient PL of exciton and trap emission in the early stage. The green arrows show the time delay of exciton and trap emission. (c) Configuration coordinate diagram of total energy (electronic + elastic energies) of conduction band (U_C), trap state (U_t), and valence band (U_V) versus single lattice coordinate Q in a semiconductor. The transition from orthorhombic to tetragonal phase makes the trap state shift in the Q space and moves the state crossing point from Q_O to Q_T, thus increasing the charge capture activation energy from $E_{B(O)}$ to $E_{B(T)}$. The equilibrium position of the trap state is consequently moved from $Q_{t(O)}$ to $Q_{t(T)}$, which directly influences the energy difference for trap emission. (d) Excitation intensity-dependent steady-state PL spectra of the perovskite at 70 K. Two main peaks corresponding to the exciton and trap emission are marked. The trap emission shows a progressive blue-shift under higher excitation intensities. (e) Logarithmic relationship between the trap PL peak and the intensity at temperatures ranging from 50 to 130 K. The minimum energy difference for the trap emission is derived by fitting to a model discussed in the supplementary material.

Within this model, following exciton trapping, the captured charges could recombine vertically according to the Franck-Condon principle to emit a photon, i.e. trap emission.[44] This has been observed by us across the whole temperature region below the phase transition. According to the configuration coordinate diagram depicted in Figure 4(c), the increase in the energy barrier E_B is expected to be accompanied by the movement of the trap emission path. The vertical energy difference (ΔE_0) between the bottom of the trap state and the valence band would in this case be increased, which should be reflected through a change in the trap PL peak energy (ΔE). However, the significant dependence between the ΔE and the excitation intensity (see Figure 4(d) and Supplementary

Figure 17) makes it difficult to directly extract the temperature-dependent ΔE_0. Through extrapolation, we find a logarithmic correlation between the ΔE and the integrated I_{PL} of the trap emission under low excitation densities of 10^{13} to 10^{16} cm^{-3} (Figure 4(e)). The modelling of trap occupation (Supplementary material note 3) provides a good fit to the experimental results and permits ΔE_0 to be readily extracted (see Figure 4(e)). For temperatures lower than 110 K, ΔE_0 is in the range of 1.64 eV and 1.66 eV, which is also directly reflected by the overlapping of the ΔE-I_{PL} plots. For 120 K to 130 K, the ΔE_0 is significantly increased to 1.72 eV and 1.77 eV, respectively. Notably, the trap emission fits indicate that the trap density and distribution have not been influenced by the phase transition, nor has the bandgap, as reflected by the same exciton emission energy (Supplementary Figure 7). Thus, the giant increase in ΔE_0 of more than 100 meV is strong evidence to support an increase in E_B and, consequently, for the multiphonon transition scenario proposed. This suggests that the charge trapping reduction with the tetragonal phase originates from the increase in the charge capture activation energy following the phase transition.

The above results suggest that the impressive long carrier lifetime that the perovskite possesses is arisen from a relatively weak electron-lattice coupling strength. This prediction about the electronic and atomic structure feature of the perovskite could give implications for the future exploration of new photoelectric materials with outstanding carrier properties. For the bound exciton, the binding energy (55 meV) to its host trap centre is much larger than that within the silicon (5-16 meV)[54], ZnO (~20 meV)[55], GaAs (~6 meV)[56] and CdS (~18 meV)[57]. This large binding energy may originate from the distinctive atomic and electronic properties of the perovskite or from Coulomb attractions from trap pairs, which helps to make the bound exciton stable at room temperature (Supplementary Figure 5 and 18) and play critical roles in practical devices. Firstly, the bound exciton could help extend the band-edge light absorption, making contributions to the photocurrent improvement of the perovskite solar cell. Secondly, the charge localization caused by the bound exciton could increase the radiative loss and thus lower the photocurrent output, especially when the built-in electric field within the perovskite absorber is weakened by the external bias voltage and internal ion redistribution. This would suppress the improvement of photovoltage and fill factor of the cell towards the Shockley-Queisser limit. Thus, for the design of efficient perovskite photovoltaic devices, the bound exciton state needs to be considered. Modifying the trap centres by composition, doping and microstructure adjustments could be a feasible route to regulate the exciton properties. Thirdly, the bound exciton is an ideal energy-level source for energy-efficient light emitting and lasing devices. The lasing originated from a bound-exciton mechanism usually has a much lower threshold compared to other mechanisms (e.g. electron-hole plasma and exciton-exciton scattering), beneficial for reducing the energy cost.[58] We have found that the bound exciton of the perovskite can be easily pumped to give a stimulated emission (Supplementary Figure 18). Further benefits of such a large exciton binding energy are envisaged for myriad applications, including optical nonlinear and bi-stable devices. Overall, the discovery of a high-temperature bound exciton would bring the excitonic feature of the lead halide perovskites to be a concern when designing efficient energy conversion and utilization devices.

Conclusions

In conclusion, the band-edge and sub-gap energy state related absorption and emission characteristics of lead halide perovskites have been systematically studied to derive the exciton and trap states and their dynamic properties. The coexistence of free and bound exciton states has been discovered in both the polycrystalline and single crystal (both surface and bulk) perovskites across a wide temperature region up to 300 K. It is found that the exciton emission and trapping processes are closely related to the trap states and exhibit a phase-dependent behaviour. In the orthorhombic phase, the excitons can be trapped within picoseconds, resulting in strong trap emission. In the tetragonal phase, this process is prohibited, yielding an ultralow trap capture cross section of 10^{-18} cm^2 and long carrier lifetime up to several hundred nanoseconds. This behaviour has been explained within the multiphonon transition theory, stemming from the increase of trap capture activation energy, likely due to a reduction of electron-lattice interaction following the orthorhombic-to-tetragonal phase transition. These findings provide a deeper insight into the distinctive photophysical properties of the class of perovskite materials, as well as provide energy state correlations to enable the development of optoelectronic devices with tailored spectroscopic signatures and, ultimately, higher performance.

Experimental Methods

Perovskite sample preparation and characterization. For the polycrystalline perovskite powder dispersion, it was formed by stabilizing the perovskite powders in the viscous ethylacetate (EA)/ethylcellulose (EC) solution. Firstly, 0.2 g ethylcellulose (Sigma-Aldrich 46060 and 46070) was dissolved in 15 ml ethylacetate by stirring at 65 °C for 1 hour in a closed bottle. For the $MAPbBr_3$ ($MAPbI_3$), 0.2 M $PbBr_2$ (PbI_2) and 0.2 M MABr (MAI) were sequentially poured into the viscous EA/EC solution under a vigorous stirring and heating. The solution became bright yellow as soon as the perovskite raw materials contacted with each other. With continuous heating and stirring, the color became darker. After 2 hours, the raw materials were completely transformed into the perovskite polycrystalline, which was evenly dispersed and stabilized in the solution. For the dilution process, 50 ml EA/EC solution was prepared at first. For a certain perovskite concentration, 1 ml 0.2 M perovskite was diluted by the pure EA/EC solution under the stirring condition. The size of the perovskite grains within the dispersion is estimated by using a light scattering method (BIC 90Plus Zeta). An optical microscope (Olympus) was also used to observe the grains by depositing the dispersion onto a glass slide.

The $MAPbBr_3$ polycrystalline film (~200 nm) was prepared by the anti-solvent method, where the quartz glass was used as the substrate. 1 M $MAPbBr_3$ dissolved in the DMF was used as the precursor. For film deposition, the $MAPbBr_3$ solution was dropped onto the substrate and spun coated at 5000 rpm, and 100 ml of chlorobenzene was dropped onto the film surface rapidly 5 s after the beginning of spin coating. The final smooth film was heat treated at 100 °C for 10 min. After that, 2 mg/ml PMMA solution

(chlorobenzene) was coated onto the film by the spin coating process.

The $MAPbBr_3$ single crystal was grown by the inverse temperature crystallization method as previously reported. Firstly, 1 M $MAPbBr_3$ solution (DMF) was prepared by the continuous stirring at room temperature for 2 h. The precursor solution was poured into a clean bottle with a diameter of about 3 cm through two series-connected 0.45 μm filters. This closed bottle was then put into the oil bath and the temperature was gradually increased and stabilized at 80 °C. After about 2 h without any disturbance, two to three small cuboid crystal nucleuses appeared. With another 2 h, the crystals grew freely and a size of several millimeters was obtained. The single crystal with a well shape was chosen as the sample, which was taken out from the bottle and put into the 2 mg/ml PMMA solution (chlorobenzene) rapidly. This single crystal was stored in the PMMA solution until used. Just before the optical measurements, the single crystal was also cleaved in the glovebox by a sharp scalpel under a certain pressure. The cutting plane is parallel to the top surface of the crystal, which is (100) plane of the cubic $MAPbBr_3$. An optical flat surface without any physical cracks can be obtained by this cleaving process. Immediately after the cleaving, the targeted crystal was re-put into the PMMA solution and then taken out for the following measurements. The structure single crystal is measured by the X-ray diffraction (Panalytical).

Optical measurements. For the possible structure relaxation, the perovskite samples, except the cleaved bulk single crystal, were kept in the dark for one day before all the optical measurements. The quartz cuvette is used to store the perovskite dispersion for light absorption measurements, which are conducted by a UV-vis spectrometer (Shimadzu 3600). The steady-state and transient PL of the perovskite dispersion, film and single crystal were all measured by the Edinburgh Fluorescence Spectrometer (FLS 920). A 445 nm pulsed diode laser (EPL-445, ~5 nJ cm^{-2}, 62 ps) was used as the excitation source. A circle adjustable neutral density filter was adopted to adjust the excitation intensity. The PL was collected by the reflectance mode, where a PMT together with a TCSPC module was applied to detect the time-resolved or time-integrated PL. For the temperature dependent measurements, an ARS liquid helium cryostat was employed as the sample chamber, where the temperature was controlled by the Lakeshore controller. The perovskite film on the glass substrate was directly fixed to the optical sample holder by screws while the single crystal was pasted to a glass substrate by the high-thermal-conductive low-temperature vacuum grease (Apiezon N). During the temperature adjustment, the system was firstly stabilized for 5 min at each temperature. Before the PL measurements, the perovskite sample was always kept in dark without any bias light or laser illumination to avoid the possible production of charge accumulation and local electric field. For the trap density measurements, a high-energy OPO laser (Opotek Vibrant, 410 nm) was used as the excitation source. A series of fixed neutral density filters and a circle adjustable neutral density filter (Zolix) were applied to adjust the pump fluence at the sample, which was calibrated by a laser energy meter (OPHIR, NOVA II). The PL was measured by a reflectance mode, which was focused into an optical fiber and collected by a CMOS spectrometer (Avantes, EVO) in a time-integrated mode.

Averaged photocharge density (n) calculations. For the trap density measurement at room temperature, the perovskite PL was measured in the pulse excitation mode, where the laser repetition time is much longer than the charge lifetime of the perovskite. Thus, the photocharge density can be estimated as n=excitation fluence each pulse/(photon energy × optical penetration depth). The PL photons are estimated to have a penetration depth of 200 nm for both the thin film and single crystal. For the observation of trap emission blue-shift at low temperature, the carrier lifetime is much longer than the laser repetition time. The perovskite film was excited in an approximately steady-state mode. Thus, a relationship exists as $G_{exc}=n/\tau_0$, where G_{exc} is the generation rate of non-equilibrium charge derived from the excitation power and τ_0 is the charge recombination lifetime.

Conflicts of interest

There are no conflicts of interest to declare.

Acknowledgements

This work was supported by the Natural Science Foundation of China (Grant Nos. 51761145042, 51372270, 11474333, 51421002, 91433205, 91733301 and 51627803). JJ would like to acknowledge funding through the ARC Centre of Excellence in Exciton Science (CE170100026).

Notes and references

1 A. Kojima, K. Teshima, Y. Shirai, T. Miyasaka, *J. Am. Chem. Soc.* **131**, 6050 (2009).
2 H. S. Kim, C. R. Lee, J. H. Im, K. B. Lee, T. Moehl, A. Marchioro, S. J. Moon, R. H. Baker, J. H. Yum, J. E. Moser, M. Grätzel, N. G. Park, *Sci. Rep.* **2**, 591 (2012).
3 M. M. Lee, J. Teuscher, T. Miyasaka, T. N. Murakami, H. J. Snaith, *Science* **338**, 643 (2012).
4 J. Burschka, N. Pellet, S. J. Moon, R. H. Baker, P. Gao, M. K. Nazeeruddin, M. Grätzel, *Nature* **499**, 316 (2013).
5 W. S. Yang, B.-W. Park, E. H. Jung, N. J. Jeon, Y. C. Kim, D. Uk Lee, S. S. Shin, J. Seo, E. K. Kim, J. H. Noh, S. Il Seok, *Science* **356**, 1376 (2017).
6 Z. Tan, R. S. Moghaddam, M. L. Lai, P. Docampo, R. Higler, F. Deschler, M. Price, A. Sadhanala, L. M. Pazos, D. Credgington, F. Hanusch, T. Bein, H. J. Snaith, R. H. Friend, *Nature Nanotech.* **9**, 687 (2014).
7 G. Xing, N. Mathews, S. S. Lim, N. Yantara, X. Liu, D. Sabba, M. Grätzel, S. Mhaisalkar, T. C. Sum, *Nat. Mater.* **13**, 476 (2014).
8 Y. Fang, Q. Dong, Y. Shao, Y. Yuan, J. Huang, *Nature Photon.* **9**, 679 (2015).
9 W. J. Yin, T. Shi, Y. Yan, *Adv. Mater.* **26**, 4653 (2014).
10 G. Xing, N. Mathews, S. Sun, S. Lim, Y. M. Lam, M. Grätzel, S. Mhaisalkar, T. C. Sum, *Science* **342**, 344-347 (2013).
11 S. D. Stranks, G. E. Eperon, G. Grancini, C. Menelaou, M. J. Alcocer, T. Leijtens, L. M. Herz, A. Petrozza, H. J. Snaith, *Science* **342**, 341 (2013).

12 Q. Dong, Y. Fang, Y. Shao, P. Mulligan, J. Qiu, J. Huang, *Science* **347**, 967 (2015).
13 N. K. Noel, A. Abate, S. D. Stranks, E. S. Parrott, V. M. Burlakov, A. Goriely, H. J. Snaith, *ACS Nano* **8**, 9815 (2014).
14 Y. Yang, D. P. Ostrowski, R. M. France, K. Zhu, J. Lagemaat, L. M. Luther, M. C. Beard, *Nat. Photon.* **10**, 53 (2016).
15 H. Zhu, K. Miyata, Y. Fu, J. Wang, P. Joshi, D. Niesner, K. W. Williams, S. Jin, X. Y. Zhu, *Science* **353**, 1409 (2016).
16 J. I. Pankove, Optical processes in semiconductors. Dover Publications: New York, 1971.
17 D. S. Chemla, D. A. B. Miller, *J. Opt. Soc. Am. B* **2**, 1155 (1985).
18 V. D'Innocenzo, G. Grancini, M. J.P. Alcocer, A. R. S. Kandada, S. D. Stranks, M. M. Lee, G. Lanzani, H. J. Snaith, A. Petrozza, *Nat. Commun.* **5**, 3586 (2014).
19 Y. Yamada, T. Nakamura, M. Endo, A. Wakamiya, Y. Kanemitsu, *J. Am. Chem. Soc.* **136**, 11610 (2014).
20 L. Luo, L. Men, Z. Liu, Y. Mudryk, X. Zhao, Y. Yao, J. M. Park, R. Shinar, J. Shinar, K. Ho, I. E. Perakis, J. Vela, J. Wang, *Nat. Commun.* **8**, 15565 (2017).
21 H. He, Q. Yu, H. Li, J. Li, J. Si, Y. Jin, N. Wang, J. Wang, J. He, X. Wang, Y. Zhang, Z. Ye, *Nat. Commun.* **7**, 10896 (2016).
22 C. Sheng, C. Zhang, Y. Zhai, K. Mielczarek, W. Wang, W. Ma, A. Zakhidov, Z. V. Vardeny, *Phys. Rev. Lett.* **114**, 116601 (2015).
23 B. Wu, H. T. Nguyen, Z. Ku, G. Han, D. Giovanni, N. Mathews, H. J. Fan, T. C. Sum, *Adv. Energy Mater.* **6**, 1600551 (2016).
24 a) S. De Wolf, J. Holovsky, S. J. Moon, P. Loper, B. Niesen, M. Ledinsky, F. J. Haug, J. H. Yum, C. Ballif, *J. Phys. Chem. Lett.* **5**, 1035 (2014). b) Z. Chen, Q. Dong, Y. Liu, C. Bao, Y. Fang, Y. Lin, S. Tang, Q. Wang, X. Xiao, Y. Bai, Y. Deng, Jinsong Huang, *Nat. Commun.* **8**, 1890 (2017).
25 T. Wang, B. Daiber, J. M. Frost, S. A. Mann, E. C. Garnett, A. Walsh, B. Ehrler, *Energy Environ. Sci.* **10**, 509 (2017).
26 E. M. Hutter, M. C. Gelvez-Rueda, A. Osherov, V. Bulovic, F. C. Grozema, S. D. Stranks, T. J. Savenije, *Nat. Mater.* **16**, 115 (2017).
27 R. H. Bube, Photoelectronic properties of semiconductors. Cambridge University Press: UK, 1992.
28 N. Ahn, K. Kwak, M. S. Jang, H. Yoon, B. Y. Lee, J. K., Lee, P. V. Pikhitsa, J. Byun, M. Choi, *Nat. Commun.* **7**, 13422 (2016).
29 D. W. deQuilettes, W. Zhang, V. M. Burlakov, D. J. Graham, T. Leijtens, A. Osherov, V. Bulović, H. J. Snaith, D. S. Ginger, S. D. Stranks, *Nat. Commun.* **7**, 11683 (2016).
30 W. Nie, J. Blancon, A. J. Neukirch, K. Appavoo, H. Tsai, M. Chhowalla, M. A. Alam, M. Y. Sfeir, C. Katan, J. Even, S. Tretiak, J. J. Crochet, G. Gupta, A. D. Mohite, *Nat. Commun.* **7**, 11574 (2016).
31 Y. Liu, Z. Yang, D. Cui, X. Ren, J. Sun, X. Liu, J. Zhang, Q. Wei, H. Fan, F. Yu, X. Zhang, C. Zhao, S. Liu, *Adv. Mater.* **27**, 5176 (2015).
32 Y. Fang, H. Wei, Q. Dong, J. Huang, *Nat. Commun.* **8**, 14417 (2017).
33 R. J. Elliott, *Phys. Rev.* **108**, 1384 (1957).
34 K. Galkowski, A. Mitioglu, A. Miyata, P. Plochocka, O. Portugall, G. E. Eperon, J. T.-W. Wang, T. Stergiopoulos, S. D. Stranks, H. J. Snaith, R. J. Nicholasc, *Energy Environ. Sci.* **9**, 962 (2016).
35 S. A. March, C. Clegg, D. B. Riley, D. Webber, I. G. Hill, K. C. Hall, *Sci. Rep.* **6**, 39139 (2016).
36 D. Priante, I. Dursun, M. S. Alias, D. Shi, V. A. Melnikov, T. K. Ng. O. F. Mohammed, O. M. Bakr, B. S. Ooi, *Appl. Phys. Lett.* **106**, 081902 (2015).
37 A. Dobrovolsky, A. Merdasa, E. L. Unger, A. Yartsev, I. G. Scheblykin, *Nat. Commun.* **8**, 34 (2017).
38 H. Fang, R. Raissa, M. Abdu-Aguye, A. Adjokatse, G. R. Blake, J. Even, M. A. Loi, *Adv. Func. Mater.* **25**, 2378 (2015).
39 M. Leroux, N. Grandjean, B. Beaumont, N. F. Semond, J. Massies, P. Gibart, *J. Appl. Phys.* **86**, 3721 (1999).
40 B. Schmidt, K. Lischks, *Phys. Rev. B* **45**, 8989 (1992).
41 H. Shibata, M. Sakai, A. Yamada, K. Matsubara, K. Sakurai, H. Tampo, S. Ishizuka, K. K. Kim, S. Niki, *Jpn. J. App. Phys.* **44**, 6113 (2005).
42 M. I. Saidaminov, A. L. Abdelhady, B. Murali, E. Alarousu, V. M. Burlakov, W. Peng, I. Dursun, L. Wang, Y. He, G. Maculan, A. Goriely, T. Wu, O. F. Mohammed, O. M. Bakr, *Nat. Commun.* **6**, 7586 (2015).
43 R. Ohmann, L. K. Ono, H. -S. Kim, H. Lin, M. V. Lee, Y. Li, N. -G. Park, Y. Qi, *J. Am. Chem. Soc.* **137**, 16049 (2015).
44 C. H. Henry, D. V. Lang, *Phys. Rev. B* **15**, 989 (1977).
45 T. Takebe, J. Saraie, H. Matsunami, *J. Appl. Phys.* **53**, 457 (1982).
46 A. D. Wright, C. Verdi, R. L. Milot, G. E. Eperon, M. A. Perez-Osorio, H. J. Snaith, F. Giustino, M. B. Johnston, L. M. Herz, *Nat. Commun.* **7**, 11755 (2016).
47 M. Karakus, S. A. Jensen, F. D'Angelo, D. Turchinovich, M. Bonn, E. Canovas, *J. Phys. Chem. Lett.* **6**, 4991 (2015).
48 F. Brivio, J. M. Frost, J. M. Skelton, A. J. Jackson, O. J. Weber, M. T. Weller, A. R. Goñi, A. M. A. Leguy, P. R. F. Barnes, A.Walsh, *Phys. Rev. B* **92**, 144308 (2015).
49 D. Niesner, M. Wilhelm, I. Levchuk, A. Osvet, S. Shrestha, M. Batentschuk, C. Brabec, T. Fauster, *Phys. Rev. Lett.* **117**, 126401 (2016).
50 K. Huang, A. Rhys, *Proc. R. Soc. A* **204**, 406-423 (1950).
51 A. Poglitsch, D. Weber, *J. Chem. Phys.* **87**, 6373 (1987).
52 A. Mattoni, A. Filippetti, M. I. Saba, P. Delugas, *J. Phys. Chem. C* **119**, 17421 (2015).
53 J. Feng, *APL. Mater.* **2**, 081801 (2014).
54 J. R. Haynes, *Phys. Rev. Lett.* **4**, 361 (1960).
55 D. C. Reynolds, D. C. Look, B. Jogai, C. W. Litton, T. C. Collins, W. Harsh, G. Cantwell, *Phys. Rev. B* **57**,12151 (1998).
56 M. A. Gilleo, P. T. Bailey, D. E. Hill, *Phys. Rev.* **174**, 898 (1968).
57 D. G. Thomas, J. J. Hopfield, *Phys. Rev.* **128**, 2135 (1962).
58 J. Ding, H. Jreon, T. Ishihara, M. Hagerott, A. V. Nurmikko, H. Luo, N. Samarth, J. Furdyna, *Phys. Rev. Lett.* **69**, 1707 (1992).

Table of contents

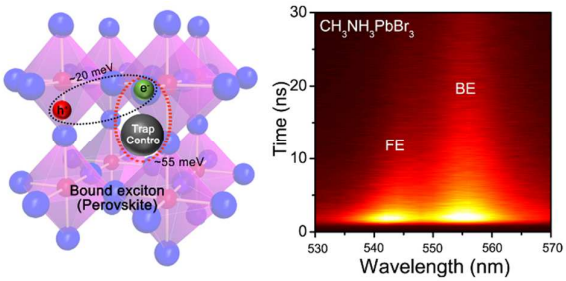

A high-temperature-stable bound exciton (BE) within the perovskite and a phase-dependent exciton trapping behaviour have been identified.

Broader context

Energy and environment have always been a hot topic for realizing a sustainable development of human societies. Perovskite solar cell, a promising candidate for energy conversion, has achieved great successes in photovoltaic performances in the past few years. This intrinsically arises from the distinctive optoelectronic properties that the perovskite material possesses as well the numerous efforts that have been paid for understanding them. It has been widely demonstrated that the hybrid lead halide perovskite is a free carrier-based semiconductor with high light absorption coefficient, ultralong hot carrier cooling and carrier recombination lifetimes. However, the material and charge characters that have a close association with the energy conversion processes are still in highly controversial. Herein, we investigate the band-edge and sub-gap energy states of the perovskite by means of temperature-, excitation intensity- and time-dependent optical measurements. The coexistence of a free and a bound exciton (with binding energy of ~70 meV) has been discovered within both the polycrystalline and single crystal perovskites across a wide temperature region up to 300 K, thus highlighting the critical roles that the exciton plays in determining the photoelectric behaviors of perovskite energy materials and devices.